Thermal activation of impedance measurements on an epoxy coating for the corrosion protection: 2. electrochemical impedance spectroscopy study

Aurélien Roggero [a], Nicolas Caussé [a], Eric Dantras [b], Laura Villareal [a, c], Audrey Santos [c], Nadine Pébère [a, *]

[a] Université de Toulouse, CIRIMAT-ENSIACET, 4 Allée Emile Monso, BP44362, 31030, Toulouse Cedex 4, France
[b] Université de Toulouse, Physique des Polymères, CIRIMAT, Université Paul Sabatier, Bât. 3R1b2, 118 Route de Narbonne, 31062, Toulouse Cedex 9, France
[c] Peintures MAESTRIA, 41 Avenue de La Rijole, 09100, Pamiers, France

A B S T R A C T

In this series, an epoxy varnish for the corrosion protection of carbon steel was analysed in the dry state by broadband dielectric spectroscopy (part 1) to describe the molecular mobility of the epoxy network. Electrochemical impedance spectroscopy (EIS) measurements were then performed in a NaCl solution (part 2), with the intent to detect the signature of the molecular mobility in the wet state. The dielectric manifestation of the glass transition (α mode), previously characterized in part 1 of this series for the dry varnish, was evidenced from EIS measurements through the use of the dielectric permittivity formalism. This α mode showed the characteristic Vogel Fulcher Tamman dependence, shifted towards higher frequencies when compared to that of the dry varnish, consistently with the plasticization of the epoxy network due to the water uptake. Moreover, it was shown that taking the α mode into account when fitting the EIS impedance data with equivalent circuits led to a much better fit in the capacitive resistive transition region. It was shown that the dc charge transport processes are not only triggered but also governed by the molecular mobility of the epoxy network. In the case of thick coatings (several hundreds of micrometers), this dependence demonstrated the absence of through pores, as it is often discussed in the literature. Indeed, under the assumption of current flowing through free electrolyte *via* open pores, the temperature dependence of the electrolyte's dc conductivity (Arrhenius law) should be found instead of the temperature dependence of molecular mobility.

Keywords:
Organic coating
Barrier property
Molecular mobility
Electrochemical impedance spectroscopy
Broadband dielectric spectroscopy

1. Introduction

In part 1 of this series, an epoxy varnish for the corrosion protection of carbon steel was studied in the dry state by means of Broadband Dielectric Spectroscopy (BDS). A comprehensive picture of the molecular mobility modes was obtained. In part 2, temperature controlled Electrochemical Impedance Spectroscopy (EIS) was used to stimulate the molecular mobility of the same epoxy varnish, whilst immersed in an electrolytic solution. The aim of part 2 is to evidence the contribution of the molecular mobility to the electrochemical impedance response, and hopefully throw light on mechanisms of corrosion protection by organic coatings.

When EIS is performed on high performance coatings that show no signs of corrosion even after several months of immersion, the Bode diagrams have a typical capacitive response over a wide range of frequencies, and sometimes a capacitive resistive transition appears for longer immersion times. From such Bode plots, three main parameters can be extracted. The first one is the low frequency impedance modulus, generally associated with the barrier property in the sense of closing the corrosion circuit. According to Mayne's work [1], the higher the modulus is, the “better” the coating is believed to be, as it limits the flow of current responsible for corrosion [2–4], even if some recent studies debate the direct relation between corrosion processes and coating resistivity [5]. The second parameter lies in the high frequency region of the impedance spectra. From the relative dielectric permittivity of the dry coating and that of water, water uptake can be calculated [6–9], allowing the study of sorption kinetics as well as the determination

* Corresponding author.
E-mail address: nadine.pebere@ensiacet.fr (N. Pébère).

https://doi.org/10.1016/j.electacta.2019.03.007

of the immersion time corresponding to water saturation. The last parameter is the transition from the high frequency capacitive behaviour to the low frequency resistive behaviour, often observed in EIS studies of coated metals and sometimes ascribed to the delamination of the polymer film [10]. This transition happens at a cut off frequency to which a film time constant reciprocally cor responds, that generally does not draw much interest from the organic coatings community.

In the present work, the epoxy varnish from part 1 of this series will be studied by EIS during immersion in a 0.5 M NaCl solution, in the temperature range [T_{room};75 °C]. The different domains of the impedance spectra described above will be analysed within the scope of dielectric properties of the epoxy network in order to determine how the molecular mobility contributes to the electro chemical impedance response in the wet state. The dielectric permittivity formalism, used in BDS, will first be applied to the EIS data to detect the signature of the molecular mobility in the immersed coating. Then, the electrical conductivity formalism will be used to emphasize the charge transport phenomena and study their temperature dependence. Finally, the conventional equivalent circuit approach will be seen under the light of dielectric relaxations.

2. Experimental

2.1. Materials

An epoxy varnish (DGEBA resin with polyaminoamide hard ener) was formulated by Peintures Maestria (Pamiers, France). The average molecular weight (Mw) of the resin was lower than 700 g/ mol. The number of epoxy groups available was 190 g/eq and that of amine/amid groups in the hardener was around 100 g/eq. The solvent was ortho xylene. This polymer matrix is representative of many commercial organic coatings in which several fillers and pigments are added to obtain the final formulation. In the present study, for the sake of simplicity, the coating was characterized for a simplified system (without inorganic fillers but diluents and plas ticizers were kept for the application with an air spray gun). The varnish was deposited by spray drying onto S235JR shot blasted steel plates. The chemical composition of the steel in weight percent was as follows: C: 0.17; Mn: 1.4; P: 0.035; S: 0.035; N: 0.012; Cu: 0.55 and Fe to the balance.

The samples were cured 21 days at 21 °C in a climate controlled curing room to allow the crosslinking process and outgassing of solvents excess. After curing, the coating was 200 ± 10 μm thick (measured by ultrasonic thickness measurement) and a glass transition temperature (T_g) of 54 ± 1 °C was measured by differ ential scanning calorimetry (at the midpoint). With a profilometer, a mean roughness of 8 μm was measured on the surface of the steel plates, which lies within the uncertainty range of the thickness measurement.

2.2. Temperature controlled electrochemical impedance spectroscopy

Electrochemical Impedance Spectroscopy (EIS) measurements were performed with a conventional three electrode cell and a REF600 + apparatus by Gamry Instruments. A REF201 Red Rod reference electrode (saturated KCl) by Radiometer Analytical was used for its wider temperature range (up to 100 °C) compared to the usual saturated calomel electrode (up to 60 °C). A graphite rod was used as counter electrode. The EIS measurements were per formed in a 0.5 M aqueous NaCl solution to reproduce seawater corrosive environment. Electrical conductivity measurements were performed on the isolated NaCl solution by using a DDS 11C benchtop conductivity meter by Sanxin.

An open bottom double jacketed cell was used to control the temperature of the electrolytic solution by means of a heated water circulation (ED 5 by Julabo). This setup allowed an accurate tem perature control (± 0.2 °C stability) over the range [T_{room};75 °C]. This range could easily be extended down to ~0 °C by using a cooling capable thermal controller. On the other hand, tempera tures above 75 °C would probably disturb EIS measurements due to convection induced currents. A fluorinated ethylene propylene (FEP) coated Pt100 sensor was used to monitor the electrolyte temperature at the interface with the coating. A battery powered Pt100 reader was used to avoid electrical perturbation of the EIS measurements. The temperature at the surface of the varnish was checked to be stable and equal to that of the electrolyte after an equilibration time of about 15 min. The temperature controlled EIS cell is represented in Fig. 1. Over the investigated temperature range, thermal expansion leads to an increase in the coating thickness which lies within the uncertainty range of the thickness measurements. In first approximation, the influence of the thermal expansion was therefore neglected in the impedance results analysis.

EIS measurements were performed in the frequency range [10^{-2};10^5 Hz] with an applied voltage of 1 V^{RMS} around the open circuit potential (8 points per decade). Typically, EIS modulation of ~30 mV are used, so as to stay within the Stern Geary linear po larization region, in the event of Faradaic processes be present. However, in the absence of corrosion processes, such a low voltage is not favourable to induce measurable dipole reactions to the applied field (*i.e.* polarization). BDS generally operates with electric fields in the order of 10^4 V/m, which are almost two decades higher than those of standard EIS measurements (10^2 V/m). For the study of organic films in EIS, increasing the applied voltage is not an issue as long as the impedance response remains linear with respect to the applied field. In this study, such linearity was checked up to 2 V^{RMS}. Finally, the use of 1 V^{RMS} modulation did not induce any additional noise or perturbation (related to the reference electrode) in the high frequency range by comparison to a 30 mV^{RMS} modulation.

2.3. Broadband dielectric spectroscopy

Broadband Dielectric Spectroscopy (BDS) experiments were performed on the dry epoxy varnish. This technique uses an impedance analyser similar to the one used in EIS. The sample is placed between two metallic electrodes and an alternative voltage (1 V of amplitude) is applied without dc bias, relative to the elec trical ground. The experimental details are reported in part 1 of this series.

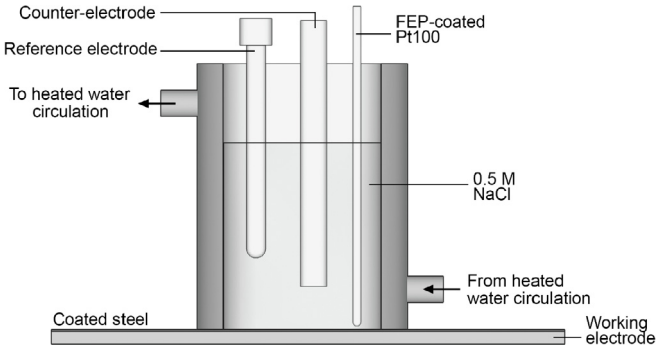

Fig. 1. Schematic diagram of the temperature-controlled EIS cell.

3. Results and discussion

3.1. Molecular mobility associated with the glass transition in EIS experiments

Temperature controlled EIS measurements were performed on the epoxy varnish after 2 weeks of immersion in a 0.5 M NaCl so lution to allow the saturation of the coating by the electrolyte (checked by monitoring the impedance modulus values at 10^5 Hz over immersion time until stabilization to a constant value). Approximately 1 wt % of water uptake at saturation was deter mined by gravimetric measurements on free standing films (results not shown). During the whole experiment, no corrosion products (*i.e.* iron oxides) could be observed by eye underneath the trans parent epoxy varnish. The impedance diagrams (Bode coordinates) obtained for the epoxy varnish in the temperature range [20; 70 °C] are shown in Fig. 2.

The diagrams seem to feature a single time constant with a transition from a resistive behaviour at low frequency (constant impedance modulus) to a capacitive behaviour at high frequency (decreasing power law of frequency). As the temperature increases, the transition is shifted towards higher frequencies, the low frequency impedance modulus significantly decreases and the frequency independent plateau broadens. The Bode plots evolution due to increasing the temperature is similar to that caused by electrolyte sorption over immersion times [11–15]. Bierwagen et al. performed analogous temperature controlled experiments in an attempt to design accelerated ageing procedures for organic coat ings and obtained comparable evolutions of the impedance modulus with temperature, when testing two space grade polymer coatings [16]. Another study by Li et al. yielded a similar evolution with an epoxy protective coating [17]. Fig. 2 shows that the impedance response of the immersed epoxy varnish is thermally activated. Similarly to how Broadband Dielectric Spectroscopy (BDS) data were treated in part 1 of this series, the dielectric permittivity formalism was applied to the impedance data so as to evidence the signature of the molecular mobility. The Bode graphical representation of the impedance data, due to the math ematical convolution of the real and imaginary components of complex impedance, is not the most appropriate for fine analysis of dielectric relaxations associated with the molecular mobility. The experimental complex impedance spectra ($Z'(\omega)$, $Z''(\omega)$) were mathematically transposed to the complex dielectric permittivity formalism ($\varepsilon'(\omega)$, $\varepsilon''(\omega)$) thanks to Eq. (1) to Eq. (3):

$$\varepsilon'(\omega) \quad \frac{Z''(\omega)}{\omega C_v (Z'(\omega)^2 + Z''(\omega)^2)} \tag{1}$$

$$\varepsilon''(\omega) \quad \frac{Z'(\omega)}{\omega C_v (Z'(\omega)^2 + Z''(\omega)^2)} \tag{2}$$

$$\text{with} \quad C_v \quad \frac{\varepsilon_v A}{l} \tag{3}$$

where ω is the angular frequency of the applied voltage and C_v the capacitance of the equivalent vacuum filled (ε_v is the vacuum permittivity) parallel plate capacitor formed by two electrodes of area A (here, the area of the EIS cell) separated by the distance l (here, the coating thickness). The dielectric permittivity is therefore an intensive property of the material, contrary to the impedance which varies with the size of the sample. Its real part, $\varepsilon'(\omega)$, is associated with energy storage (conservative phenomena) while its imaginary part, $\varepsilon''(\omega)$, relates to the dissipative phenomena inducing energy losses. Such losses can arise from either electrical charge carrier transport or molecular mobility modes (involving dipoles that are constitutive of the macromolecule). The calculated real permittivity spectra obtained from the EIS measurements are shown in Fig. 3. The inset in Fig. 3 shows the BDS real permittivity spectra obtained on the dry varnish in the temperature range [50; 100 °C] and already described in part 1 of this series.

There are obvious similarities in the EIS (wet) and BDS (dry) responses as both of them feature permittivity steps as well as a steep rise in the real permittivity at low frequencies and high temperatures. The latter is ascribed to electrode polarization effects

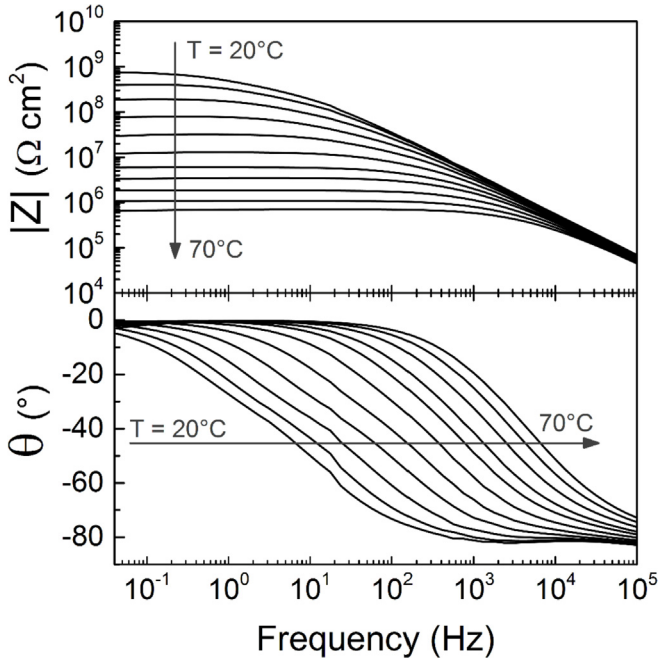

Fig. 2. Bode plots of the isothermal EIS measurements performed on the epoxy varnish after 2 weeks of immersion in a 0.5 M NaCl solution. The temperature step between each curve is 5 °C. For the sake of readability, the 8 experimental points per decade are represented as continuous lines.

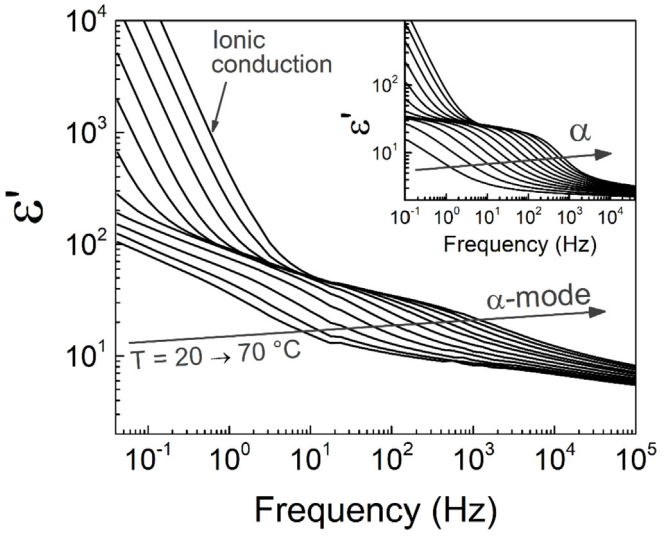

Fig. 3. Isothermal relative permittivity spectra (real part of ε*) obtained from the EIS measurements on the epoxy varnish (2 weeks of immersion in 0.5 M NaCl). Inset: BDS spectra of the dry epoxy varnish, in the temperature range [50; 100 °C]. For the sake of readability, the 8 experimental points per decade are represented as continuous lines.

due to an accumulation of charge carriers at the electrode interfaces, resulting in a macroscopic dipole able to preferentially orient along the applied electric field only at low frequencies [18].

In dielectric studies of polymers molecular mobility, a step in ε' is generally attributed to the conservative manifestation of a dipole relaxation *i.e.* a molecular mobility mode [19]. In the inset of Fig. 3, these steps are clearly ascribed to the α mode that is the dielectric manifestation of the glass transition (extensively studied in part 1 of this series). When the polymer is exposed to an alternating electric field, the dipoles constitutive of the macromolecule slightly move (over angles of a few degrees at most) in an attempt to align themselves with the applied field. There is a temperature (and equivalently a frequency) at which these motions generate the most dielectric losses (that can be seen as molecular friction). Above and below the maximum, dielectric losses decline, leading to a dielectric relaxation (in the form of a loss peak) associated with a molecular mobility mode. In particular, the α mode corresponds to the molecular mobility gained at the glass transition. The steps observed in the EIS real permittivity spectra (Fig. 3), similarly to the BDS results, might also correspond to the α mode of the epoxy network. In order to confirm this assumption, the temperature dependence of the EIS real permittivity steps was analysed. For that, a determination method of the relaxation times associated with the permittivity steps was needed. As an example, the real and imaginary parts of the dielectric permittivity obtained from EIS measurements are shown in Fig. 4 for the 55 °C isotherm. While a step in $\varepsilon'(\omega)$ is clearly visible, its associated dissipative peak is deeply buried in the conductivity rise of $\varepsilon''(\omega)$. The Kramers Kronig transform algorithm by Steeman and Van Turnhhout [20] was used to recalculate the imaginary part of the complex permittivity, $\varepsilon''_{K\text{-}K}(\omega)$, from $\varepsilon'(\omega)$, in order to minimize the purely dissipative contributions of the charge transport. In the $\varepsilon''_{K\text{-}K}(\omega)$ spectrum, as a substantial part of the charge transport contribution has been removed from $\varepsilon''(\omega)$, a relaxation peak becomes clearly distinguishable, but not enough to extract an unequivocal relaxation time (typically by fitting the Havriliak Negami equation as in part 1). Finally, the dielectric loss factor, $\tan\delta_{K\text{-}K}(\omega)$, was calculated as in Eq. (4):

$$\tan\delta_{K-K}(\omega) \quad \frac{\varepsilon''_{K-K}(\omega)}{\varepsilon'(\omega)} \tag{4}$$

The $\tan\delta_{K\text{-}K}(\omega)$ spectrum now allows unambiguous determination of a unique time constant τ_{max} corresponding to the maximum of the peak (indicated by the dotted line in Fig. 4).

In Fig. 5 are reported the real permittivity (ε') and $\tan(\delta_{K\text{-}K})$ isothermal spectra obtained in BDS and EIS at 55 °C. The α mode is clearly identified as a step in permittivity and a peak in $\tan(\delta_{K\text{-}K})$ for both the dry and immersed coatings. The shift towards higher frequencies observed for the immersed coating (EIS) is ascribed to the expected plasticization of the epoxy network by the absorbed water [21]. The molecular mobility of the immersed, plasticized network, benefits from the disruption of intra and intermolecular physical bonds due to water interaction. Molecular motions involved in the α mode therefore happen at a higher frequency, or with a smaller relaxation time, than in the much more physically bonded dry network.

The relaxation times of the supposed α mode were extracted from all the EIS isothermal $\tan\delta_{K\text{-}K}(\omega)$ spectra and are displayed in Fig. 6 along with those of the dry varnish obtained from BDS measurements. Both curves mainly obey the Vogel Fulcher Tammann (VFT) law [22–24] as is generally expected for the dielectric manifestation of the glass transition (due to cooperative molecular mobility) [25]:

$$\tau(T) \quad \tau_0^{VFT} e^{\frac{1}{\alpha_f (T - T_\infty)}} \tag{5}$$

where T is the temperature, τ_0^{VFT} a pre exponential factor, T_∞ the Vogel temperature and α_f the thermal expansion coefficient of free volume, which can be defined as the difference between the volumetric thermal expansion coefficients of the polymer well above and well below T_g, the glass transition temperature ($\alpha_{vol}^{T \gg T_g} - \alpha_{vol}^{T \ll T_g} + \alpha_f$) [26 p:48].

As a side note, the EIS relaxation times seem to have two temperature dependences below and above [30–40 °C]. In Fig. 6, the three first points on the low temperature side seem to be linear (emphasized by the dotted line), corresponding to an Arrhenius dependence. These points have therefore not been considered for the VFT fit. Such change of behaviour suggests that the α mode thermal activation is different on both sides of T_g (measured at 37 °C by DSC for the wet varnish). This phenomenon has been

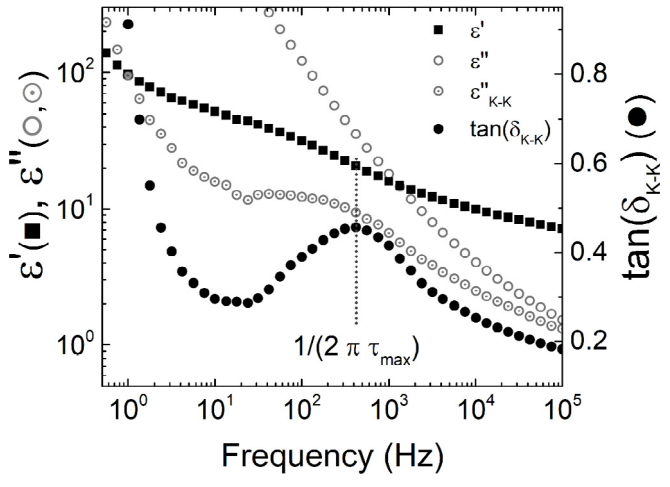

Fig. 4. Real (■) and imaginary (○) parts of the dielectric permittivity obtained from the EIS data at T 55 °C, as well as the Kramers-Kronig recalculated imaginary component (⊙) and associated loss factor $\tan(\delta_{K\ K})$ (●). The dotted line indicates the position of the time constant τ_{max} determined at the maximum of the $\tan(\delta_{K\ K})$ peak.

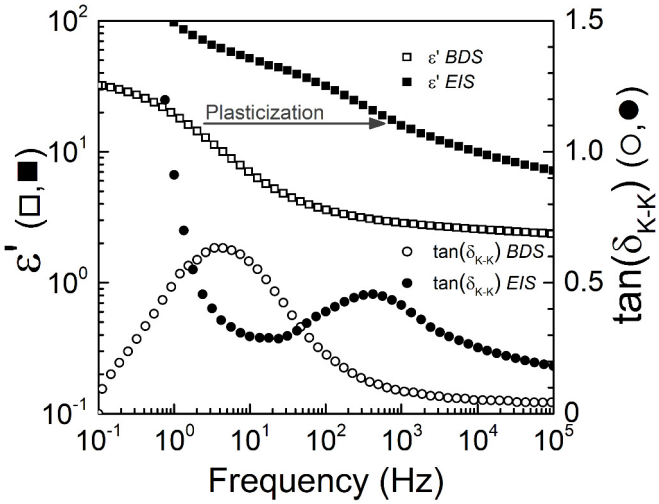

Fig. 5. Real permittivity, ε' (□,■), and $\tan(\delta_{K\ K})$ (○,●) from BDS (dry epoxy varnish) and EIS (immersed epoxy varnish) measurements at T 55 °C. The arrow indicates the plasticizing effect of absorbed water.

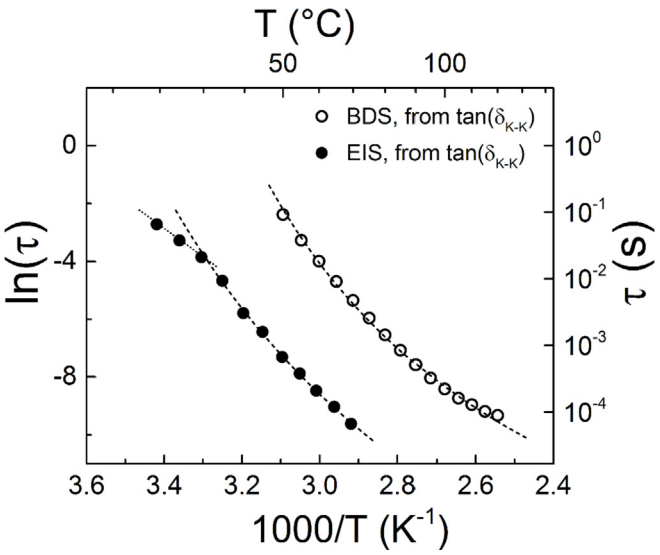

Fig. 6. Arrhenius plot of the time constants determined at the maximum of tan($\delta_{K\ K}$) for the BDS (○) and EIS (●) measurements. The VFT fits are represented in dashed lines and the dotted line serve as a guide for the eye.

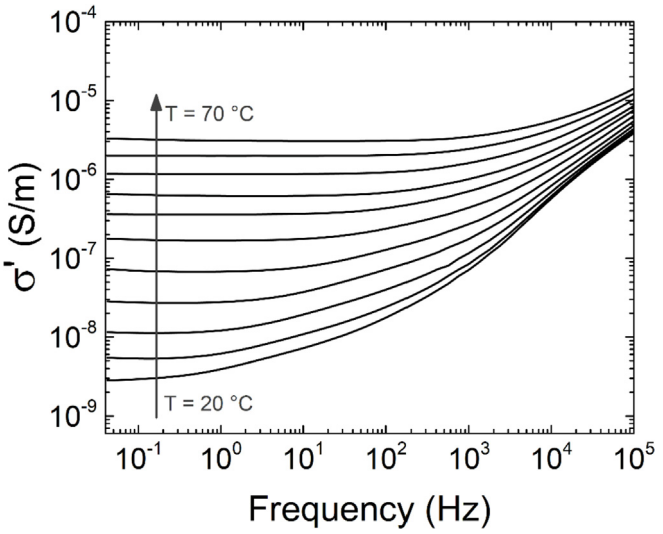

Fig. 7. Real part of the electrical conductivity calculated from the isothermal EIS measurements performed on the immersed epoxy varnish (2 weeks of immersion in 0.5 M NaCl).

reported for small molecules [27] but never in polymer materials with practical applications and with a unique experimental tech nique. Studies coupling BDS and thermally stimulated depolariza tion currents (TSDC) reported that the α mode evolved from a VFT dependence at higher frequencies (BDS in the rubbery state) to an Arrhenius dependence at lower frequencies (TSDC in the glassy state) [28]. In our case, the heavily plasticized state of the epoxy network in EIS could possibly allow observing this crossover with a single technique.

The VFT fit parameters of the dry (BDS measurements) and immersed (EIS measurements) epoxy varnish are reported in Table 1. The pre exponential factor τ_0^{VTF} varies over two decades between the dry and wet varnish, but no physical interpretation is generally given to this parameter in the literature. The other two fit parameters share the same order of magnitude and are consistent with the plasticization by the absorbed water. In particular, the decrease of T_∞ for the wet varnish is consistent with the shift to wards lower temperatures of the relaxation times, as observed in Fig. 6. Both the VFT dependence of the relaxation times and the consistency of the fit parameters under the plasticization hypoth esis confirmed that the signature of molecular mobility can be observed in EIS measurements.

3.2. Temperature dependence of the electrical conductivity for the immersed varnish

The experimental impedance data from BDS and EIS measure ments were converted to the electrical conductivity formalism by means of Eq. (6) and Eq. (7), to emphasize the charge transport processes. The isothermal conductivity spectra are represented in Fig. 7.

Table 1
Vogel-Fulcher-Tammann fit parameters for the α-mode of the dry (BDS) and immersed (EIS) epoxy varnish.

	τ_0^{VTF} (s)	α_f (K ^{1})	T_∞ (K)
Dry (tan($\delta_{K\ K}$))	(5.1 ± 0.3) 10 ^{8}	(1.0 ± 0.2) 10 ^{3}	254 ± 8
Immersed (tan($\delta_{K\ K}$))	(6.5 ± 0.7) 10 ^{10}	(7.3 ± 0.3) 10 ^{4}	224 ± 14

$$\sigma^*(\omega) \quad \sigma'(\omega) + i\sigma''(\omega) \quad i\,\omega\,\varepsilon_v\varepsilon^*(\omega) \tag{6}$$

$$\sigma'(\omega) \quad \omega\,\varepsilon_v\varepsilon''(\omega) \tag{7}$$

where ε_v is the vacuum permittivity.

The immersed coating (EIS) features low frequency dc con duction plateaus where σ' is independent of frequency. These pla teaus are followed by a power law of frequency at higher frequencies, in agreement with the "universal dielectric relaxation response" [29] of disordered materials, defined by Jonscher (Eq. (8), discussed in part 1 of this series). Observing this response in a polymer coating saturated with water suggests that it should not be treated differently to any non crystalline material. To confirm this point of view, an analysis of the temperature dependence of the dc conductivity is needed.

$$\sigma'(\omega) \quad \sigma_{dc} + A\omega^s \tag{8}$$

where σ_{dc} is the dc conductivity value, A a constant, ω the angular frequency and s a non ideality exponent for the high frequency power law (with $0 < s < 1$).

The temperature dependence of the dc conductivity is plotted in Fig. 8 as a function of reciprocal temperature (Arrhenius plot), for both the dry (BDS measurements) and wet (EIS measurements) epoxy varnishes, as well as for the isolated 0.5 M NaCl solution. The latter has a high electrical conductivity (10^2–10^3 S/m) and an Arrhenius dependence on temperature, with a low activation en ergy of 0.12 eV. The dc conductivity of the dry sample is 10–13 orders of magnitude lower than that of the electrolyte, indicating the insulating nature of this polymer. Moreover, its temperature dependence obeys a VFT law with activation parameters similar to the α mode of the molecular mobility.

The dc conductivity of the immersed sample, obtained from EIS, are also reported in Fig. 8. They are by three orders of magnitude higher than those of the dry varnish, which confirms the substan tial contribution of absorbed water to the ion hopping conductivity processes in the coating. However, this contribution does not impact the temperature dependence of electrical conductivity, which mainly displays VFT dependence very similar to that of the

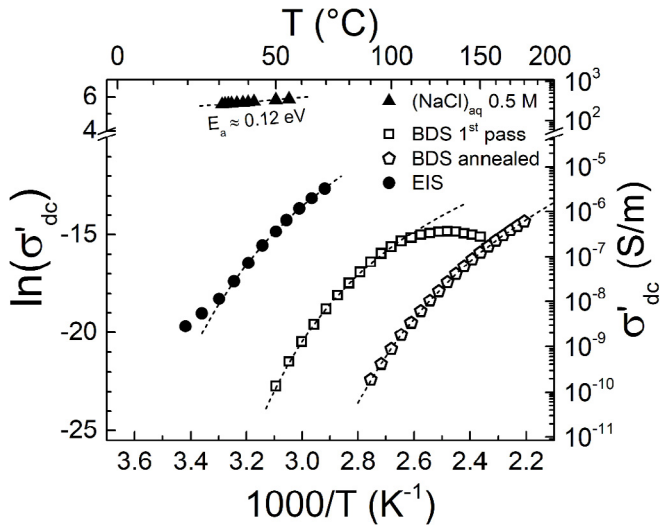

Fig. 8. Arrhenius diagram of the dc conductivity (real part of σ* taken on the frequency-independent plateaus) from EIS (2 weeks of immersion in 0.5 M NaCl) and BDS (dry) measurements on the epoxy varnish.

dry sample. The VFT fit parameters are reported in Table 2 for the dc conductivity of the dry and wet coatings.

Generally, no physical interpretation is given to the pre exponential factor σ_0^{VTF}. The free volume thermal expansion coef ficient, α_f, of both samples is within error margins, in good agree ment with the same apparent curvatures observed in Fig. 8. The 24 K lower T_∞ for the immersed varnish is also consistent with the plasticization of the α mode discussed in section 3.1. The conser vation of the VFT dependence for the immersed varnish suggests that the mechanism (ion hopping processes) at the microscopic scale remains the same, and that it is characteristic of a polymer in interaction with water rather than of "free" electrolytic solution through open pores in the material. The pore resistance concept, where pores are defined as direct electrical pathways to the sub strate through continuous macroscopic defects (or free volume) filled with electrolytic solution, is often found in studies related to organic coatings [30–33]. The presence of such pores in polymers (especially in thick films) is debatable [34], while the characteristic size of free volume (in the order of 0.1 nm^3 [35]) seems too small and discontinuous to contain liquid like electrolytic solution. If the "pores scenario" was valid for polymer coatings, then the electrical conductivity of the wet varnish should display an Arrhenius dependence on temperature with an activation energy close to that of the isolated NaCl solution (0.12 eV), only with lower conductivity values due to the reduction in the section available for the elec trolyte (the paths through pores). Therefore, in the present work, the obtained VFT dependence rather suggests that the charge transport occurs through the polymer as a medium, which, under the prominent influence of water, is directly involved in the charge transport processes. This statement seems consistent with the concepts developed by Mayne et al., who proposed that network heterogeneity at the microscopic scale leads to the existence of pathways of least resistance through the polymer coating, correlated with easier electrolyte absorption [36]. One could argue that such heterogeneity is constitutive of polymers and results, at the macroscopic scale, in distributions (as opposed to discrete values) of physical parameters (permittivity, conductivity), the measured value of which being an average (or centre) of the dis tribution. This discussion about through pores should however be tempered in the case of thin organic coatings (a few to a few tens of μm in thickness) where any defect formed during the application might behave like an open pore.

Table 2
Vogel-Fulcher-Tammann fit parameters for the dc conductivity of the dry and immersed epoxy varnish.

	σ_0^{VTF} (S m ^{1})	α_f (10^{-3} K^{-1})	T_∞ (K)
Dry (BDS)	$(5.6 \pm 0.3)\ 10^{-4}$	(1.2 ± 0.1)	266 ± 3
Immersed (EIS)	$(3.1 \pm 0.5)\ 10^{-2}$	(1.1 ± 0.1)	242 ± 4

3.3. Equivalent circuit approach

The use of the dielectric permittivity formalism allowed the signature of the molecular mobility in the EIS response of the immersed epoxy varnish to be shown. The aim of this section is to determine how the α mode can be accounted for in an equivalent circuit.

The R//CPE equivalent circuit, consisting of a constant phase element (non ideal capacitance) in parallel with an ideal resistor, is very popular among the organic coatings community [37–39]. The equivalent complex impedance of the R//CPE circuit is described by Eqs. (9) and (10).

$$Z^*_{R//CPE} \quad \frac{R}{1 + (j\omega)^{\alpha_{CPE}} R\,Q} \tag{9}$$

$$\tau_{R//CPE} \quad (RQ)^{\frac{1}{\alpha_{CPE}}} \tag{10}$$

where R is a resistor, ω the angular frequency of the applied voltage, Q a parameter with physically meaningless units of $F.s^{(\alpha-1)}$ and α_{CPE}, related to the non ideality of the capacitor replaced by a CPE, equals the constant phase angle divided by π/2.

The EIS response of organic coatings is often fitted with a R//CPE circuit and the parameters R, Q and α_{CPE} are monitored over im mersion time. The R//CPE behaviour has been analysed and modelled by taking into account distributions of the electrical re sistivity along the sample thickness, due to an inhomogeneous electrolyte uptake [40–43]. As pointed out by West et al. [44], the universal Jonscher's law, Eq. (8), is equivalent to a R//CPE circuit: the non ideality power law exponent from Eq. (8), s, corresponds to the CPE exponent, α_{CPE}. The Jonscher's law is universally observed in any disordered solid, from inorganic glasses to polymers, regardless of their water content. Therefore, in the case of organic coatings, ascribing a R//CPE behaviour strictly to water uptake seems debatable from the start, even if the non ideality exponent may be influenced by water sorption.

The R//CPE parameters were graphically determined [45] from the isothermal EIS impedance modulus spectra (Fig. 2). For three of them, the obtained R//CPE fits are reported (dashed lines) in Fig. 9.

The impedance modulus was considered in Ω rather than Ω cm^2, usually found in the literature (*e.g.* in Fig. 2). Normalizing the modulus with the respect to the EIS cell area while not accounting for the coating thickness shows its limitation when it comes to the construction of equivalent circuits. Although the fits in Fig. 9 ac count for the global frequency dependence of the impedance modulus, they are not satisfying in the capacitive resistive transi tion region, where Eq. (9) fails. This is particularly noticeable in the phase angle diagrams, where the R//CPE fits show transitions that are too spread when compared to the experimental data. The un derlying presence of the α mode is assumed to induce an additional phase dispersion in the capacitive resistive transition region and the simple R//CPE equivalent circuit is not able to take it into ac count. A dielectric relaxation that has only one non ideality parameter, α_{cc} $(0 \leq \alpha_{cc} < 1)$, related to the spread, can be

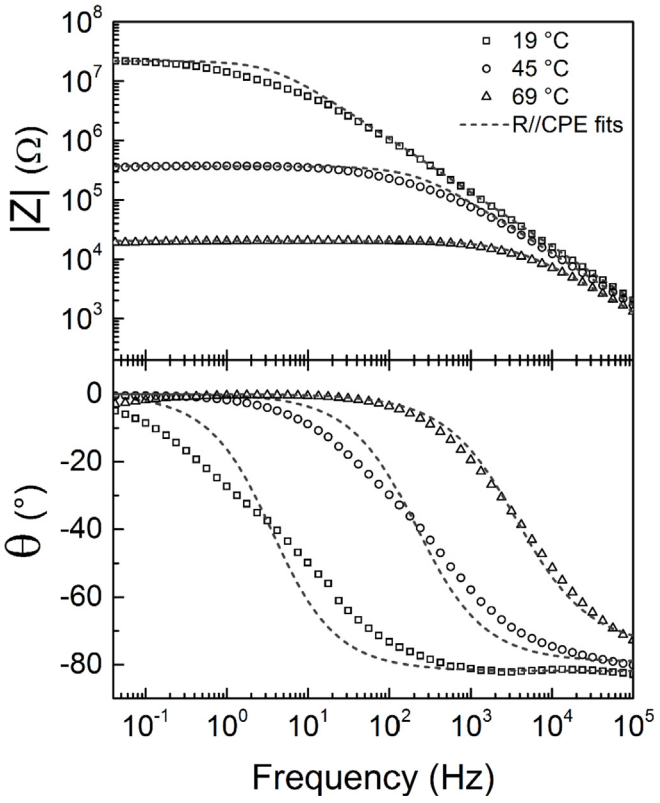

Fig. 9. Bode plots of 3 isothermal EIS measurements performed on the epoxy varnish (2 weeks of immersion in 0.5 M NaCl) and R//CPE equivalent circuit fits.

modelled by the Cole Cole equation [46], which is equivalent to the Havriliak Negami equation with $\beta_{H\text{-}N}$ 1 (see Eq. (4) from part 1 of this series). The choice of the Cole Cole relaxation in this section, rather than the more versatile Havriliak Negami equation, was motivated by the difficulty in translating the second spread parameter, $\beta_{H\text{-}N}$, to an equivalent circuit. The equivalent circuit of a Cole Cole dielectric relaxation [46] is reported in Fig. 10 with a resistor, R, added in parallel.

The vacuum filled cell capacity, C_v, defined in Eq. (3), is the link between intensive properties, such as the permittivity, ε, and extensive properties, such as the capacitance, C, or resistance, R. The two capacitances, C_s and C_∞, placed in the two branches of the Cole Cole circuit, model the step in the material permittivity ($\Delta\varepsilon$ ε_s ε_∞), observed as a consequence of the dielectric relaxation (α mode here). The Cole Cole impedance, Z_{cc}, relates to the energy

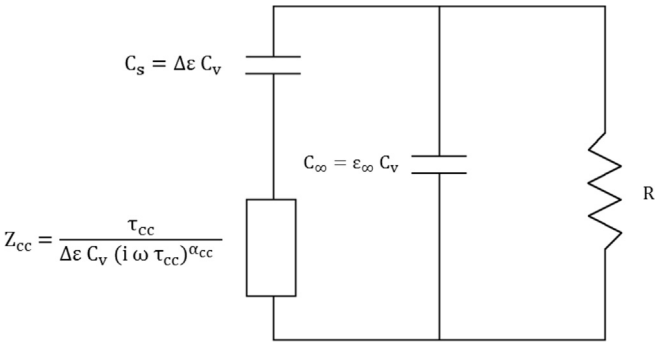

Fig. 10. Cole-Cole//R equivalent circuit consisting of a Cole-Cole relaxation with a resistor, R, in parallel.

dissipated during the dielectric relaxation. With α_{cc}, it also accounts for the non ideal distribution of the relaxation times, associated with the heterogeneity of the dipoles environment. Here, τ_{cc} cor responds to the mean dipole relaxation time of the α mode (which in dielectric studies is determined by fitting permittivity spectra with the Havriliak Negami or Cole Cole equations).

To model the low frequency conductivity (modulus plateaus in the Bode plots), a resistor R can be added in parallel [47] to the Cole Cole equivalent circuit (Fig. 10). The Cole Cole partial circuit cor responds to the dielectric relaxation (α mode) and the partial cir cuit [R,C_∞] is a simple parallel RC with a time constant τ_{RC} R C_∞ corresponding to the onset of dc conduction. The reciprocal equivalent impedance of this Cole Cole//R circuit, $1/Z^*_{eq}$, equals the sum of the reciprocal impedances of each parallel branch:

$$\frac{1}{Z^*_{eq}} \quad \sum \frac{1}{Z^*_i} \quad \frac{1}{R} + i\,\omega\,\varepsilon_\infty C_v + \frac{1}{\frac{1}{i\,\omega\,\Delta\varepsilon\,C_v} + \frac{\tau_{cc}}{\Delta\varepsilon\,C_v\,(i\,\omega\,\tau_{cc})^{\alpha_{cc}}}} \qquad (11)$$

The EIS complex impedances of the immersed epoxy varnish were fitted with Eq. (11). The Cole Cole parameters were initialized with typical values for the α mode (see section 3.1 and part 1 of this series): ε_s is in the order of a few tens, ε_∞ in the order of 3 and τ_{cc} highly depends on temperature. The 45 °C isotherm is reported in Fig. 11, along with the global Cole Cole//R fit and the isolated con tributions of the Cole Cole and [R,C_∞] parts. The other EIS iso therms were also fitted (not presented here) and the following observations apply to all of them.

Comparing Fig. 11 with the R//CPE fits (Fig. 9) shows that the Cole Cole//R equivalent circuit much better accounts for the spread of the capacitive resistive transition (particularly noticeable in the

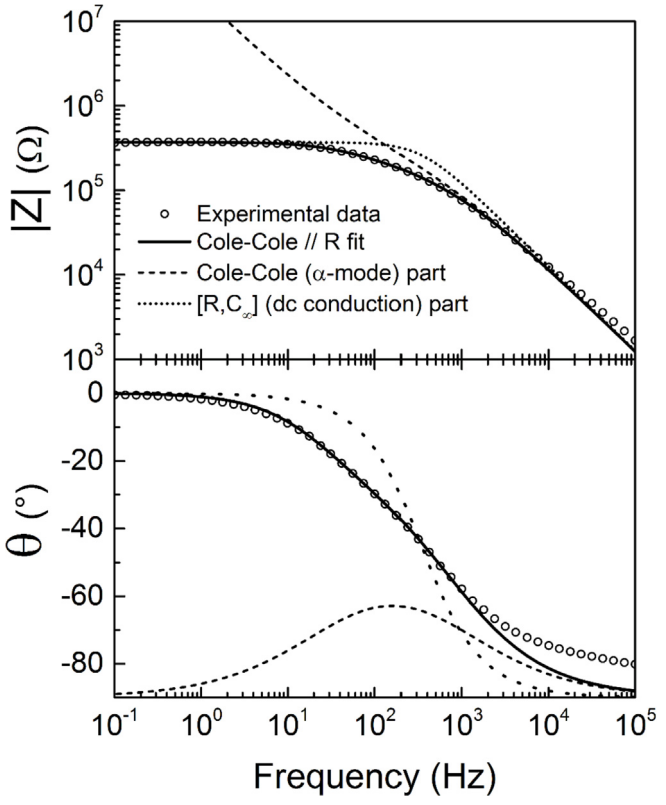

Fig. 11. Bode plot of the 45 °C EIS isotherm, performed on the epoxy varnish (2 weeks of immersion in 0.5 M NaCl). The Cole-Cole//R equivalent circuit fit is represented in solid line and the isolated contributions of the two components in dashed and dotted lines.

phase angle plots). The phase angle of the Cole Cole circuit (dashed line in Fig. 11) corresponds to the dielectric losses associated with the α mode of the epoxy network, in the form of a peak that is responsible for the spread of the global response. The [R,C_∞] circuit accounts for the low frequency impedance modulus plateau and the general shape of a low pass filter. Because C_∞ is an ideal capacitor, the [R,C_∞] circuit behaves like an ideal parallel RC. This causes a failure of the fit at high frequencies (above 10^3 Hz), which is the only region where the R//CPE fit is better than the Cole Cole// R, thanks to the α_{CPE} parameter. As mentioned earlier, the universal Jonscher's law translates to a R//CPE circuit. To take into account the Jonscher's behaviour at high frequencies, in Fig. 7, the equivalent circuit should therefore feature a CPE. It could be replacing C_∞ (which would in turn impact the Cole Cole element) or added in parallel, as suggested by other authors [44,48]. In any case, the equivalent circuit would better fit the experimental data at high frequencies, but would feature an additional non ideality parameter, difficult to ascribe to a physical phenomenon.

The same fitting procedure was applied to the BDS data of the dry epoxy varnish and reported for the 70 °C isotherm in Fig. 12, as an example. While the immersion of the varnish (electrolyte absorption) results in highly convoluted α mode and dc conduction contributions (Fig. 11), they are much more separated in the dry varnish. The good agreement between BDS data and the Cole Cole// R circuit, on top of the satisfying fit of the EIS data, confirms the validity of the equivalent circuit used. The Cole Cole//R fit parameters are reported in Table 3 for EIS (45 and 70 °C) and BDS (70 °C) measurements. These parameters should be considered as rough estimates, due to the high degree of convolution in the impedance spectra (especially with the EIS results and the failure of the fit at high frequencies). For more accuracy, the values extracted from the

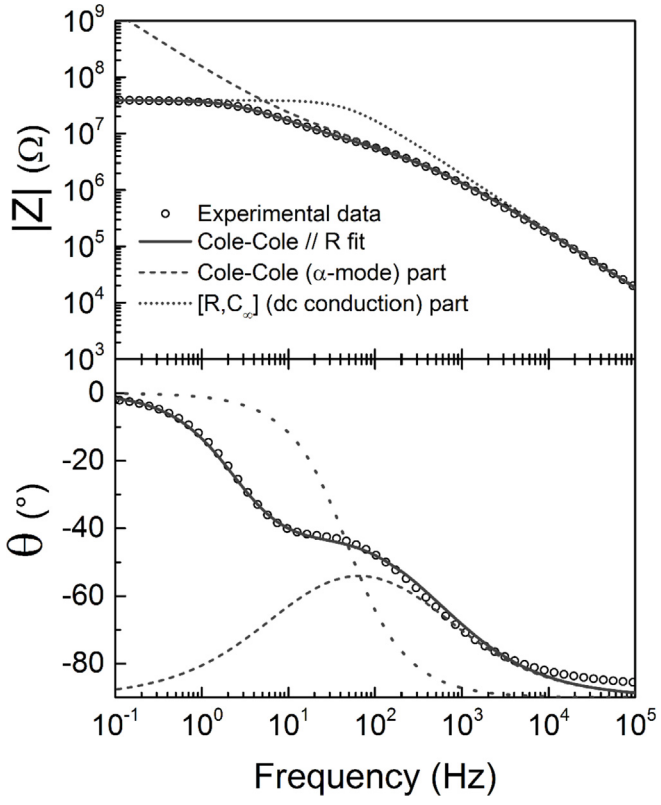

Fig. 12. Bode plot of the 70 °C BDS isotherm performed on the dry epoxy varnish. The Cole-Cole//R equivalent circuit fit is represented in solid line and the isolated contributions of the two components in dashed and dotted lines.

Table 3
Cole-Cole//R fit parameters for the immersed (45 and 70 °C) and dry (70 °C) varnish.

	EIS (45 °C)	EIS (70 °C)	BDS (70 °C)
C_v (10^{-11} F)	14.2	14.2	3.3
ε_s	74 ± 2	34 ± 2	36 ± 1
ε_∞	8.1 ± 0.2	7.7 ± 0.5	2.6 ± 0.3
τ_{cc} (10^{-3} s)	8.1 ± 0.5	0.13 ± 0.02	17.8 ± 0.9
α_{cc}	0.43 ± 0.01	0.39 ± 0.03	0.35 ± 0.05
R (10^4 Ω)	37.37 ± 0.03	2.03 ± 0.02	3888 ± 72

manipulation of intensive parameters should always be preferred (*e.g.* Fig. 3 for ε_∞ values). Nevertheless, all the parameters from Table 3 have physically reasonable values, to the slight exception of ε_s which is often difficult to estimate when low frequency charge transport has a capacitive response (ion transport), like in the case of this epoxy varnish. In particular, the high frequency permittivity limit, ε_∞, is higher with the EIS data, due to the contribution of absorbed water.

4. Conclusions

An epoxy varnish representative of the typical organic coating for the corrosion protection of carbon steel was studied with the objective of identifying the contribution of the molecular mobility on its electrochemical impedance response. By performing EIS measurements at various constant temperatures and by applying the dielectric permittivity formalism to the impedance data, the signature of the molecular mobility (α mode, dielectric manifestation of the glass transition) was evidenced in the impedance response of the varnish immersed in NaCl solution, in good agreement with the dry varnish, studied in part 1 of this series. Plasticization by absorbed water is responsible for a significant shift of this manifestation of the molecular mobility towards lower temperatures, consistently with the decrease in the calorimetric glass transition temperature. It is anticipated that temperature controlled EIS could bring insights in the molecular mobility of many protective organic coatings as a majority of them have a glass transition in the vicinity of 50 °C, which fits in the temperature range of the technique developed in the present work. Over long immersion times, such studies could evidence the influence of plasticization or ageing of the polymer matrix, which as a result directly impact the coatings performance against corrosion.

Analysing the temperature dependence of the low frequency conductivity led to the conclusion that the wet coating behaves like the plasticized dry coating. Electrolyte uptake in the epoxy network increases the dc conductivity by three orders of magnitude but the latter is still governed by the mobility of polymer sequences. The signature of the molecular mobility (Vogel Fulcher Tammann law) on the dc conductivity of the immersed epoxy varnish pointed out the absence of through pores, which are often proposed in the literature to describe the electrolyte uptake and impedance response of organic coatings.

With this particular epoxy system, the molecular mobility in the impedance spectra was accounted for by fitting a Cole Cole//R equivalent circuit. This method is not as precise as the use of intensive formalisms such as the dielectric permittivity when it comes to determining the associated relaxation times, but it was able to detect the α mode of molecular mobility, highly convoluted in the charge transport processes. It is therefore anticipated that in many other coatings, the α mode may be hidden in the impedance response.

This study confirms that taking into account the molecular mobility of a polymer based paint is necessary when assessing their barrier properties. This is generally done by performing

temperature dependent measurements, which was proven possible with EIS. It is hoped that this new experimental and analytical procedure could help better define the concept of “barrier prop erty”, by applying it to a wide range of protective organic coatings, over a wide range of temperature and frequency.

References

[1] J.E.O. Mayne, The mechanism of the protection of iron and steel by paint, Anti-corrosion Methods & Mater. 20 (1973) 3 8, https://doi.org/10.1108/eb006930.

[2] R.C. Bacon, J.J. Smith, F.M. Rugg, Electrolytic resistance in evaluating protective merit of coatings on metals, Ind. Eng. Chem. 40 (1948) 161 167.

[3] A. Amirudin, D. Thierry, Application of electrochemical impedance spectroscopy to study the degradation of polymer-coated metals, Prog. Org. Coating 26 (1995) 1 28, https://doi.org/10.1016/0300-9440(95)00581-1.

[4] M. Kendig, D.J. Mills, An historical perspective on the corrosion protection by paints, Prog. Org. Coating 102 (2017) 53 59, https://doi.org/10.1016/j.porgcoat.2016.04.044.

[5] J.M. Sykes, E.P. Whyte, X. Yu, Z. Sharer Sahir, Does “coating resistance” control corrosion? Prog. Org. Coating 102 (2017) 82 87, https://doi.org/10.1016/j.porgcoat.2016.04.015.

[6] A.S. Nguyen, N. Causse, M. Musiani, M.E. Orazem, N. Pébère, B. Tribollet, V. Vivier, Determination of water uptake in organic coatings deposited on 2024 aluminium alloy: comparison between impedance measurements and gravimetry, Prog. Org. Coating 112 (2017) 93 100, https://doi.org/10.1016/j.porgcoat.2017.07.004.

[7] D.M. Brasher, A.H. Kingsbury, Electrical measurements in the study of immersed paint coatings on metal. I. Comparison between capacitance and gravimetric methods of estimating water-uptake, J. Appl. Chem. 4 (1954) 62 72, https://doi.org/10.1002/jctb.5010040202.

[8] J.M. Sykes, A variant of the Brasher-Kingsbury equation, Corros. Sci. 46 (2004) 515 517, https://doi.org/10.1016/j.corsci.2003.10.001.

[9] A.S. Castela, A.M. Simoes, An impedance model for the estimation of water absorption in organic coatings. Part I: a linear dielectric mixture equation, Corros. Sci. 45 (2003) 1631 1646, https://doi.org/10.1016/S0010-938X(03)00014-3.

[10] C.H. Tsai, F. Mansfeld, Determination of coating deterioration with EIS: Part II. Development of a method for field testing of protective coatings, Corrosion 49 (1993) 726 737, https://doi.org/10.5006/1.3316106.

[11] Z. Sharer Sahir, J.M. Sykes, Effect of temperature on the impedance response of coated metals, Prog. Org. Coating 77 (2014) 2039 2044, https://doi.org/10.1016/j.porgcoat.2014.02.009.

[12] Y. Dong, Q. Zhou, Relationship between ion transport and the failure behavior of epoxy resin coatings, Corros. Sci. 78 (2014) 22 28, https://doi.org/10.1016/j.corsci.2013.08.017.

[13] Q. Zhou, Y. Wang, Comparisons of clear coating degradation in NaCl solution and pure water, Prog. Org. Coating 76 (2013) 1674 1682, https://doi.org/10.1016/j.porgcoat.2013.07.018.

[14] N. Fredj, S. Cohendoz, S. Mallarino, X. Feaugas, S. Touzain, Evidencing antagonist effects of water uptake and leaching processes in marine organic coatings by gravimetry and EIS, Prog. Org. Coating 67 (2010) 287 295, https://doi.org/10.1016/j.porgcoat.2009.11.001.

[15] Q. Le Thu, H. Takenouti, S. Touzain, EIS characterization of thick flawed organic coatings aged under cathodic protection in seawater, Electrochim. Acta 51 (2006) 2491 2502, https://doi.org/10.1016/j.electacta.2005.07.049.

[16] G.P. Bierwagen, L. He, J. Li, L. Ellingson, D.E. Tallman, Studies of a new accelerated evaluation method for coating corrosion resistance thermal cycling testing, Prog. Org. Coating 39 (2000) 67 78, https://doi.org/10.1016/S0300-9440(00)00106-5.

[17] J. Li, C.S. Jeffcoate, G.P. Bierwagen, D.J. Mills, D.E. Tallman, Thermal transition effects and electrochemical properties in organic coatings: Part 1 initial studies on corrosion protective organic coatings, Corrosion 54 (1998) 763 771, https://doi.org/10.5006/1.3284797.

[18] D.L. Sidebottom, B. Roling, K. Funke, Ionic conduction in solids: comparing conductivity and modulus representations with regard to scaling properties, Phys. Rev. B 63 (2000), https://doi.org/10.1103/PhysRevB.63.024301, 024301.

[19] F. Kremer, A. Schonhals, 2 broadband dielectric measurement techniques, in: F. Kremer, A. Schonhals (Eds.), Broadband Dielectr. Spectrosc., Springer-Verlag, Berlin, 2002, pp. 35 57.

[20] P.A.M. Steeman, J. Van Turnhout, A numerical Kramers-Kronig transform for the calculation of dielectric relaxation losses free from Ohmic conduction losses, Colloid Polym. Sci. 275 (1997) 106 115.

[21] S. Duval, M. Keddam, M. Sfaira, A. Srhiri, H. Takenouti, Electrochemical impedance spectroscopy of epoxy-vinyl coating in aqueous medium analyzed by dipolar relaxation of polymer, J. Electrochem. Soc. 149 (2002) B520, https://doi.org/10.1149/1.1512667.

[22] H. Vogel, The law of the relation between the viscosity of liquids and the temperature, Phys. Z. 22 (1921) 645 646.

[23] G.S. Fulcher, Analysis of the recent measurements of the viscosity of glasses, J. Am. Ceram. Soc. 8 (1925) 339 355, https://doi.org/10.1111/j.1151-2916.1925.tb16731.x.

[24] G. Tammann, W. Hesse, Die Abhangigkeit der Viscositat von der Temperatur bie unterkühlten Flüssigkeiten, Z. Anorg. Allg. Chem. 156 (1926) 245 257.

[25] F. Kremer, A. Schonhals, 4 the scaling of the dynamics of glasses and supercooled liquids, in: F. Kremer, A. Schonhals (Eds.), Broadband Dielectr. Spectrosc., Springer-Verlag, Berlin, 2003, pp. 99 129, https://doi.org/10.1007/978-3-642-56120-7_4.

[26] J.L. Halary, F. Lauprêtre, L. Monnerie, Polymer Materials: Macroscopic Properties and Molecular Interpretations, Wiley, Hoboken, 2011.

[27] S.P. Bhardwaj, R. Suryanarayanan, Use of dielectric spectroscopy to monitor molecular mobility in glassy and supercooled trehalose, J. Phys. Chem. B 116 (2012) 11728 11736, https://doi.org/10.1021/jp303317p.

[28] L. Delbreilh, E. Dargent, J. Grenet, J.-M. Saiter, A. Bernès, C. Lacabanne, Study of poly(bisphenol A carbonate) relaxation kinetics at the glass transition temperature, Eur. Polym. J. 43 (2007) 249 254, https://doi.org/10.1016/j.eurpolymj.2006.09.019.

[29] A.K. Jonscher, The “universal” dielectric response, Nature 267 (1977) 673 679. https://doi.org/10.1038/267673a0.

[30] J.M. McIntyre, H.Q. Pham, Electrochemical impedance spectroscopy; a tool for organic coatings optimizations, Prog. Org. Coating 27 (1996) 201 207, https://doi.org/10.1016/0300-9440(95)00532-3.

[31] A. Miszczyk, K. Darowicki, Accelerated ageing of organic coating systems by thermal treatment, Corros. Sci. 43 (2001) 1337 1343, https://doi.org/10.1016/S0010-938X(00)00156-6.

[32] F. Mansfeld, C.H. Tsai, Determination of coating deterioration with EIS: I. Basic relationships, Corrosion 47 (1991) 958 963, https://doi.org/10.5006/1.3585209.

[33] H.M. Ha, A. Alfantazi, On the role of water, temperature, and glass transition in the corrosion protection behavior of epoxy coatings for underground pipelines, J. Coat. Technol. Res. 12 (2015) 1095 1110, https://doi.org/10.1007/s11998-015-9705-0.

[34] G.K. Van Der Wel, O.C.G. Adan, Moisture in organic coatings - a review, Prog. Org. Coating 37 (1999) 1 14, https://doi.org/10.1016/S0300-9440(99)00058-2.

[35] H. Schmitz, F. Müller-Plathe, Calculation of the lifetime of positronium in polymers via molecular dynamics simulations, J. Chem. Phys. 112 (2000) 1040 1045, https://doi.org/10.1063/1.480627.

[36] J.E.O. Mayne, Corrosion, in: L. Shreir, R.A. Jarman, G.T. Burstein (Eds.), The Mechanism of the Protective Action of Paints, third ed., Butterworth-Heinemann, Oxford, 1994 https://doi.org/10.1016/B978-0-08-052351-4.50110-2, 14:22-14:38.

[37] E.P.M. van Westing, G.M. Ferrari, J.H.W. de Wit, The determination of coating performance with impedance measurements-I. Coating polymer properties, Corros. Sci. 34 (1993) 1511 1530, https://doi.org/10.1016/0010-938X(93)90245-C.

[38] M.E. Orazem, I. Frateur, B. Tribollet, V. Vivier, S. Marcelin, N. Pebere, A.L. Bunge, E.A. White, D.P. Riemer, M. Musiani, Dielectric properties of materials showing constant-phase-element (CPE) impedance response, J. Electrochem. Soc. 160 (2013) C215 C225, https://doi.org/10.1149/2.033306jes.

[39] F. Deflorian, L. Fedrizzi, S. Rossi, P.L. Bonora, Organic coating capacitance measurement by EIS: ideal and actual trends, Electrochim. Acta 44 (1999) 4243 4249, https://doi.org/10.1016/S0013-4686(99)00139-5.

[40] L. Young, Anodic Oxide Films Part 4. The interpretation of impedance measurements on oxide coated electrodes on niobium, Science 135 (1961) 783 784, https://doi.org/10.1126/science.135.3506.783-a.

[41] B. Hirschorn, M.E. Orazem, B. Tribollet, V. Vivier, I. Frateur, M. Musiani, Constant-phase-element behavior caused by resistivity distributions in films I, Theory, J. Electrochem. Soc. 157 (2010) C452, https://doi.org/10.1149/1.3499564.

[42] B. Hirschorn, M.E. Orazem, B. Tribollet, V. Vivier, I. Frateur, M. Musiani, Constant-phase-element behavior caused by resistivity distributions in films II. Applications, J. Electrochem. Soc. 157 (2010) C458, https://doi.org/10.1149/1.3499565.

[43] C.A. Schiller, W. Strunz, The evaluation of experimental dielectric data of barrier coatings by means of different models, Electrochim. Acta 46 (2001) 3619 3625, https://doi.org/10.1016/S0013-4686(01)00644-2.

[44] A.R. West, D.C. Sinclair, N. Hirose, Characterization of electrical materials, especially ferroelectrics, by impedance spectroscopy, J. Electroceram. 1 (1997) 65 71, https://doi.org/10.1023/A:1009950415758.

[45] M.E. Orazem, B. Tribollet, 17. Preliminary graphical methods, in: Electrochem. Impedance Spectrosc., first ed., John Wiley & Sons, Hoboken, NJ, USA, 2008, pp. 332 351, https://doi.org/10.1002/9780470381588.ch17.

[46] K.S. Cole, R.H. Cole, Dispersion and absorption in dielectrics I. Alternating current characteristics, J. Chem. Phys. 9 (1941) 341 351, https://doi.org/10.1063/1.1750906.

[47] G. Williams, D.K. Thomas, Phenomenological and molecular theories of dielectric and electrical relaxation of materials, Novocontrol Appl. Note Dielectr. 3 (1998) 1 29.

[48] M.A. Hernández, N. Masó, A.R. West, On the correct choice of equivalent circuit for fitting bulk impedance data of ionic/electronic conductors, Appl. Phys. Lett. 108 (2016), https://doi.org/10.1063/1.4946008.